Journal of Geodynamics 135 (2020) 101695

Contents lists available at ScienceDirect

Journal of Geodynamics

journal homepage: www.elsevier.com/locate/jog

A Multiple 1D Earth Approach (M1DEA) to account for lateral viscosity variations in solutions of the sea level equation: An application for glacial isostatic adjustment by Antarctic deglaciation

R. Hartmann[a,*], J. Ebbing[a], C.P. Conrad[b]

[a] Institute of Geoscience, Kiel University, Kiel, Germany
[b] Center for Earth Evolution and Dynamics (CEED), University of Oslo, Oslo, Norway

ARTICLE INFO

Keywords:
Sea level change
Uplift rates
GIA modeling
3D Earth rheology
Antarctic ice loss
Elastic lithosphere
Upper mantle viscosities
Rotational feedback
SELEN

ABSTRACT

The pseudo-spectral form of the sea level equation (SLE) requires the approximation of a radially-symmetric visco-elastic Earth. Thus, the resulting predictions of sea level change (SLC) and glacial isostatic adjustment (GIA) often ignore lateral variations in the Earth structure. Here, we assess the capabilities of a Multiple 1D Earth Approach (M1DEA) applied to large-scale ice load components with different Earth structures to account for these variations. In this approach the total SLC and GIA responses result from the superposition of individual responses from each load component, each computed globally assuming locally-appropriate 1D Earth structures. We apply the M1DEA to three separate regions (East Antarctica, West Antarctica, and outside Antarctica) to analyze uplift rates for a range of Earth structures and different ice loads at various distances. We find that the uplift response is mostly sensitive to the local Earth structure, which supports the usefulness of the M1DEA. However, stresses transmitted across rheological boundaries (e.g., producing peripheral bulges) present challenges for the M1DEA, but can be minimized under two conditions: (1) If the considered time period of ice loading for each component is consistent with the relaxation time of the local Earth structure. (2) If the load components can be subdivided according to the scale of the lateral variations in Earth structure. Overall, our results indicate that M1DEA could be a computationally much cheaper alternative to 3D finite element models, but further work is needed to quantify the relative accuracy of both methods for different resolutions, loads, and Earth structure variations.

1. Introduction

Accurate models of glacial isostatic adjustment (GIA) are essential for inferring present-day ice loss measurements and sea level changes from geodetic observations. It has been widely established that predicting sea level change (SLC) related to current and past melting events, and the associated GIA of the solid Earth, can be accomplished using the pseudo-spectral form of the sea level equation (SLE) (Mitrovica and Peltier, 1991), based on the sea level theory of Farrell and Clark (1976). Advanced formulations account for the feedback of a rotating Earth (Milne and Mitrovica, 1998), grounding line migration, and shoreline migration (Milne et al., 1999; Kendall et al., 2005), all of which increase the accuracy of the predictions. But since the spectral solutions to the SLE require the approximation of a radially-symmetric visco-elastic Earth, these predictions cannot include lateral variations in Earth structure (e.g., Peltier et al., 2015; Martin-Español et al., 2016).

Most regional models account for a 3D Earth structure by using a spatial form of the SLE in a finite element approach (Nield et al., 2018), which is computationally costly when applied on a global scale. A different approximation, recently used for GIA models of Greenland (Khan et al., 2016) and Antarctica (Sasgen et al., 2017, 2018), computes the GIA response to deglaciation in each regional basin separately, and sums the contributions. These individual GIA computations utilize different spherically-symmetric (1D) Earth structures, each chosen to be locally-appropriate for the basin that they represent. Their results suggest that such a "Multiple 1D Earth Approach" (M1DEA) can increase the accuracy of the predictions for SLC rates and GIA uplift rates compared to approaches based on a single 1D Earth structure. However, no detailed sensitivity analysis for such an approach is yet available. Thus, it is still undetermined where the M1DEA improves GIA models with lateral variations in viscosity or where the neglected interaction of the individual Earth structures degrades such GIA models. For example,

* Corresponding author. Now at: Physics of Fluids Group, University of Twente, Enschede, The Netherlands.
E-mail address: r.hartmann@utwente.nl (R. Hartmann).

https://doi.org/10.1016/j.jog.2020.101695
Received 8 July 2019; Received in revised form 9 December 2019; Accepted 12 January 2020
Available online 24 January 2020
0264-3707/

the long wavelength response to local loading or global effects like the rotational feedback (RFB) have not been characterized for M1DEA models.

Antarctica provides an appropriate setup to analyze the capabilities of the M1DEA on large-scale load components, as East and West Antarctica differ geologically (e.g., Harley et al., 2013) and in their lithospheric (e.g., An et al., 2015) and viscosity structures (e.g., van der Wal et al., 2015).

In this paper, we explore the impact of variations in Earth structure on local uplift rates for loads at various distances, with a focus on Antarctic deglaciation. Based on these results, we provide a preliminary assessment of the applicability of M1DEA to account for lateral variations in Earth's rheology structure. While our results focus on the impact of lateral variations as implemented in M1DEA, our discussion uses their implications to motivate further investigations, especially future tests between M1DEA and full 3D models.

2. Multiple 1D Earth Approach (M1DEA)

The redistribution of mass by surface loads affects the equipotential sea surface (also defined as the Geoid) and the solid surface of the Earth. The local difference of both displacements describes the SLC (e.g., Mitrovica and Peltier, 1991; Milne and Mitrovica, 1998):

$$S(\vartheta, \varphi, t) = O(\vartheta, \varphi, t)\cdot[N(\vartheta, \varphi, t) - U(\vartheta, \varphi, t)] \quad (1)$$

Here, N is the deformation of the geoid, U is the radial displacement of the solid Earth, and S is the resulting SLC. ϑ, φ, and t denote longitude, latitude, and time, respectively. O is the ocean function (Munk and MacDonald, 1960), which limits the sea level to oceanic regions.

In the pseudo-spectral form of the SLE the predicted deformations $\Psi = \{S, U, N\}$ and their corresponding rates $\psi = \{s, u, n\} = \partial_t \Psi$ are linear to the applied load L. Thus, total present-day rates are the superposition of all rates induced by the different regional components of the ice load using the same global 1D Earth model (Fig. 1(a)):

$$\psi_{\overline{1D}}(\vartheta, \varphi, t, \sum_{reg} L_{reg}) = \sum_{reg} \psi_{\overline{1D}}(\vartheta, \varphi, t, L_{reg}) \quad (2)$$

Here, the subscript reg indicates the various regional load components, which are applied individually. The subscript $\overline{1D}$ denotes the global 1D Earth structure. In order to account for lateral variations, the Multiple 1D Earth Approach (M1DEA) uses a specific regional 1D Earth structure $1D_{reg}$ for each regional load component (Fig. 1(b)):

$$\psi_{M1DEA}(\vartheta, \varphi, t, \sum_{reg} L_{reg}) = \sum_{reg} \psi_{1D_{reg}}(\vartheta, \varphi, t, L_{reg}) \quad (3)$$

In the M1DEA approximation, each 1D Earth structure is applied globally for a given load, even though it may not be valid away from the regional load. Hence, the combined rates at any point contain the contributions of multiple relaxation behaviors from all Earth structures at that point. Our preinvestigation (see Appendix B: Fig. B.1) shows that the uplift rate in each region is mostly dominated by the local loading and that the effect of loading in regions at great distances is generally small. This implies that variations in the Earth structure of distant regions should have a minor effect as well (Fig. 1(c)). Aware of the inherent inaccuracy of the M1DEA, we evaluate the capabilities of this approach in this paper. The first step is to study the effect of large-scale variations between entire ice sheets, although the M1DEA can be used for small-scale variations as well.

We calculate the various predictions of SLC S, ground surface displacement U, and sea surface displacement N, and their corresponding present-day rates $\psi = \{s, u, n\}$, using a modified version of *SELEN* 2.9.12 (Spada and Stocchi, 2007; Spada et al., 2012, 2015). This open

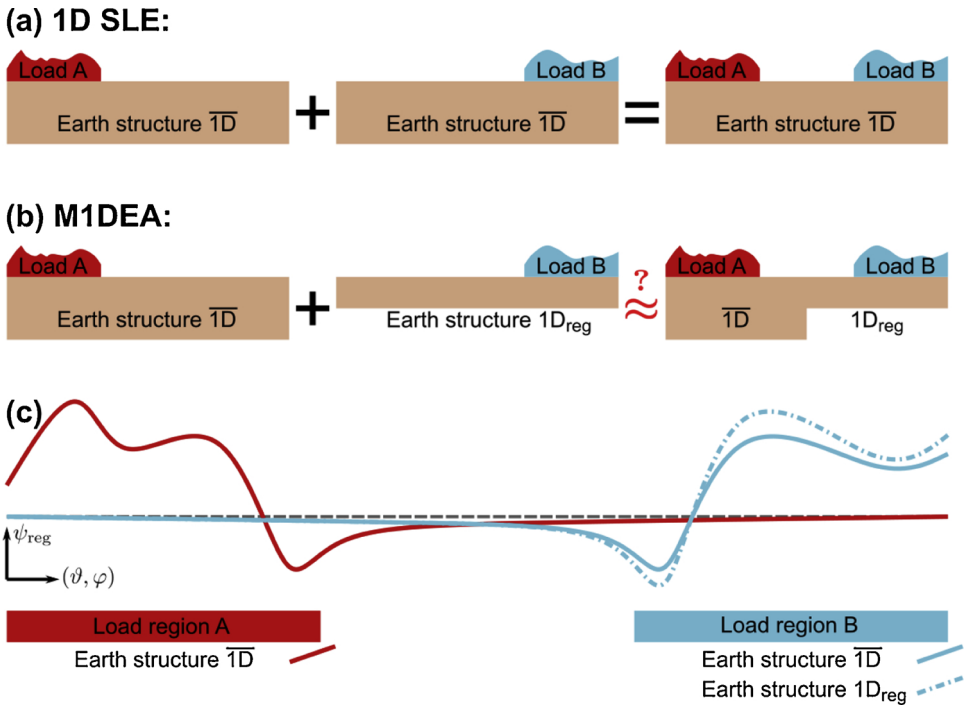

Fig. 1. (a) "Standard" solution to the 1D SLE: A sketch of the superposition of load components A (red) and B (blue) each sitting above the same radially-symmetric average Earth structure $\overline{1D}$ (Eq. (2)), (b) Idea of the M1DEA: A sketch of the superposition of load components A (red) and B (blue) on different radially-symmetric Earth structures $\overline{1D}$ and $1D_{reg}$, each describing the local structure beneath the load components A and B, respectively (Eq. (3)), (c) Schematic rates (e.g., rates of uplift) induced by the load component A on the average Earth $\overline{1D}$ (solid red line), the load component B on the average Earth $\overline{1D}$ (solid blue line), and the load component B on the regional Earth $1D_{reg}$ (dashed blue line). The M1DEA approximation works under the assumption that the induced rates are largest in the region of the corresponding load component (red and blue areas) and decrease outside this region. For the M1DEA, it is thus required that changes in the Earth structure beneath region B mostly only affect rates for region B, and not (much) for region A as well. (For interpretation of the references to color in this figure legend, the reader is referred to the web version of this article.)

source software package is based on the pseudo-spectral SLE (Mitrovica and Peltier, 1991) for an incompressible, non-rotating Earth with fixed shorelines. Further, water expulsion is not considered. However, we have modified the code to consider the rotational feedback (RFB) of the rotating Earth (Milne and Mitrovica, 1998; Mitrovica et al., 2001, 2005). Details on the implementation and the availability of the modified code can be found in Appendix C. This is done to investigate the effect of the M1DEA on global features like the RFB in addition to the local loading response. The calculations truncate the SLE at spherical harmonic degree $l_{max} = 128$, which gives a sufficient resolution for our aim – the assessment of the M1DEA for large-scale variations in the Earth structure. All numerical parameters of *SELEN*, which are used for all calculations, are summarized in Table A.1.

3. Test cases for the M1DEA

The SLE in *SELEN* basically depends on two physical quantities, the applied load and a 1D visco-elastic structure of the Earth. Here, we briefly introduce first the Earth structures and ice loading scenarios used for analysis of Earth structure variations, and afterwards our sensitivity analysis itself.

3.1. Earth structures

All tests use an Earth structure with a general setting of six layers: the core, the lower mantle (LM), the transition zone (TZ), the deep upper mantle (DUM), the shallow upper mantle (SUM), and the elastic lithosphere (EL) (Table A.2). The Earth structure defines the density ρ, the shear modulus G, and the viscosity μ of these layers, which are time-independent as *SELEN* assumes an incompressible Earth and does not include stress-dependent terms. The density and shear moduli within each layer are averaged values based on the PREM model (Dziewonski and Anderson, 1981), and only the core is assumed to be inviscid with a shear modulus set to $G = 0$ and a viscosity of $\mu = 0$. Furthermore, the basal depths of the mantle layers are fixed and the lithosphere is treated as purely elastic.

Common 1D Earth structures for SLC or GIA predictions are the global structure VM5a (Peltier and Drummond, 2008) and the optimum Earth model of the W12 GIA model (Whitehouse et al., 2012b). These Earth structures typically use viscosities around $\mu = 10^{21}$ Pa s in the upper mantle and $\mu \in [10^{21.5}, 10^{22}]$ Pa s in the lower mantle. Such a relatively stiff Earth structure is represented in our tests by the Earth structure $W12_{earth}$ (Fig. 2, blue line). Recent estimates predict very low viscosities in the upper mantle for several regions of West Antarctica (Barletta et al., 2018; Zhao et al., 2017; Nield et al., 2014). We follow the optimal model of Barletta et al. (2018) in the upper mantle together with a lower mantle viscosity of $\mu = 10^{21.5}$ Pa s (Fig. 2, red line) to represent such a low-viscosity Earth structure.

Upper mantle viscosities vary across orders of magnitude. In order to determine their impact on local uplift rates, we test 192 different combinations over a large range of upper mantle viscosities and elastic thicknesses (Fig. 2: gray zone, Table A.3). This allows for an individual analysis of viscosity and EL variations.

3.2. Load components

The results shown are calculated using the long-term loading scenario ICE-6G_C (Argus et al., 2014; Peltier et al., 2015) (hereafter ICE-6G) subdivided into several regional components. Since *SELEN* cannot account for shoreline and grounding line migration, we corrected the total ice thicknesses of the ICE-6G data for marine-grounded ice by the present-day bathymetry ETOPO (Amante and Eakins, 2009) outside Antarctica and BEDMAP2 (Fretwell et al., 2013) within the Antarctic region. The correction scheme is documented in Appendix A (Eq. (A.1), Fig. A.1, Table A.4).

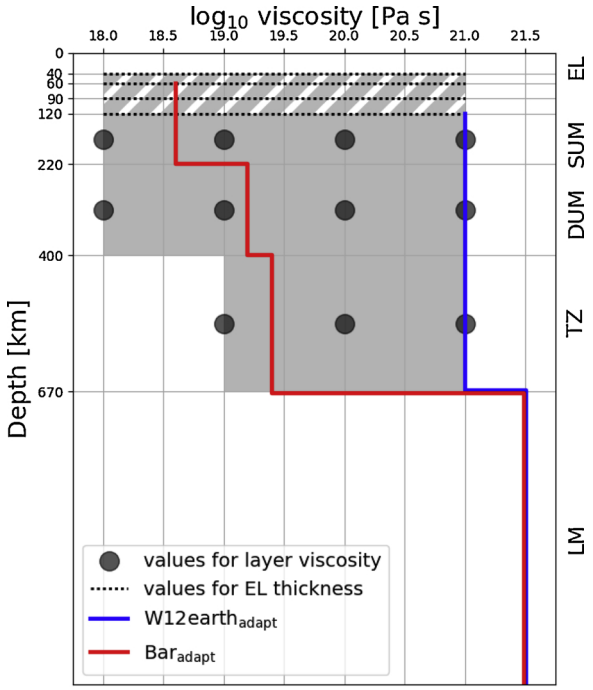

Fig. 2. Applied viscosity profiles: The colored lines show the profiles for the specific tests applied. The dark gray dots represent the different considered values for the viscosities of the upper mantle layers in the sensitivity analysis. The covered range is shaded in lighter gray. The gray and white shaded portion illustrates the range that can be viscous or elastic depending on the chosen EL thickness. The explicit values for all Earth structures are summarized in Table A.3. (For interpretation of the references to color in this figure legend, the reader is referred to the web version of this article.)

Far-distant variations

We split ICE-6G at a latitude of 60°S into an Antarctic component ICE-6ant and a Non-Antarctic component ICE-6far (Fig. 3). ICE-6far is then dominated by the ice volume change in the northern hemisphere. These two components are used to determine the impact of viscosity and EL variations at great distances from the locations of predicted uplift.

Near-distant variations

The impact of the local variations of viscosity and EL are explored for neighboring regions East and West Antarctica. Here, we additionally divide the Antarctic component of the long-term scenario ICE-6G into an East Antarctic component ICE-6eant and a West Antarctic component ICE-6want (Fig. 3). In addition to the analysis for long-term loading (ICE-6G), we define the loading scenarios $WANT_{el}$ and $WANT_{100}$ to include the effect of present and most recent ice loss in the sensitivity analysis. Therefore, we approximate the present-day ice loss in West Antarctica with $165\,\frac{Gt}{yr}$ and a constant present-day ice balance for East Antarctica ($\pm\ 0\,\frac{Gt}{yr}$), according to several estimates (Jacob et al., 2012; The IMBIE team, 2018; Chen et al., 2009; Rignot et al., 2008). This corresponds to an eustatic sea level change of $\approx 0.46\,\frac{mm}{yr}$. The West Antarctic ice loss is uniformly distributed over the present-day area of the West Antarctic region for consistency with separation of the long-term components. The loading scenario $WANT_{100}$ assumes a century of this rate of ice loss before present. The loading scenario $WANT_{el}$ is a one-year scenario with melting at the present rate.

3.3. Sensitivity analysis

We define the specific impact due to a particular Earth structure variation beneath a given region of loading as following: Assume ice

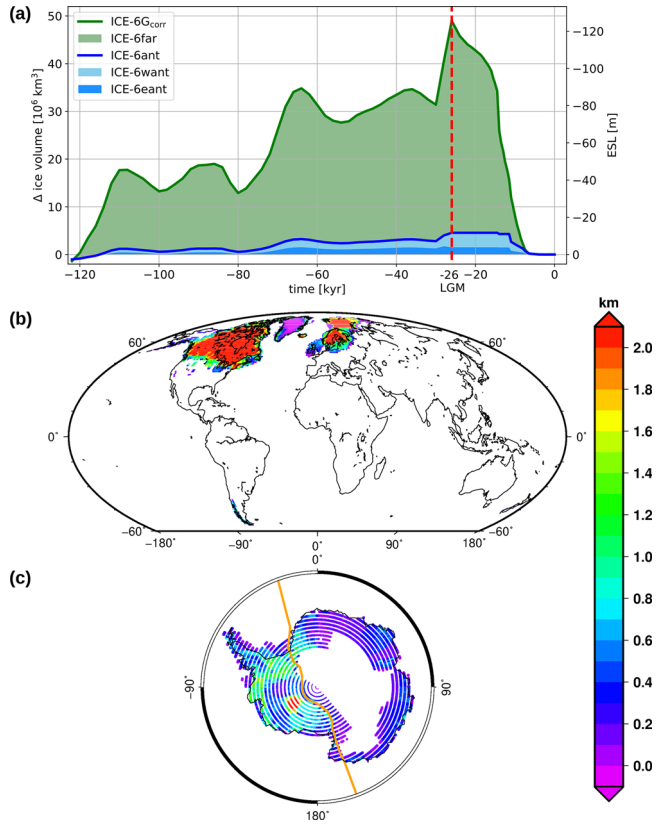

Fig. 3. (a) Ice volume of the corrected loading scenario ICE-6G referenced to the present state (zero loading at $t = 0$). The global volume (green line) is divided into the specific components (color shaded zones). The Antarctic component (blue line) consists of the East and West Antarctic components (blue shaded zones). The red line indicates the last glacial maximum (LGM). The right scale indicates the eustatic sea level (ESL) relative to the present state. (b) Ice extent at the LGM relative to the present state for the ICE-6far component. (c) Ice extent at the LGM relative to the present state for the ICE-6ant component. The orange line marks the border between the East and West Antarctic components. (For interpretation of the references to color in this figure legend, the reader is referred to the web version of this article.)

load in region B is modeled with an Earth structure v, and ice load in region A (outside B) is modeled with an Earth structure w. The impact caused by the varied structure v on the predicted rates $\psi = \{s, u, n\}$ is the difference $\Delta\psi$ between the predicted M1DEA rates and the predictions using only Earth structure w:

$$\Delta\psi = \psi_{\mathrm{M1DEA}} - \psi_{\mathrm{homog}} = (\psi_{A,w} + \psi_{B,v}) - (\psi_{A,w} + \psi_{B,w}) = \psi_{B,v} - \psi_{B,w} \tag{4}$$

The (globally defined) difference $\Delta\psi$ is expected to be large in region B, where the M1DEA rates account for the varying structure v. However, the area of interest is region A, where the M1DEA rates include the changed contribution from load component B with Earth structure v. Small differences $\Delta\psi$ in region A imply a low impact of the Earth structure v in region B on the rates in region A, which would indicate a good applicability for the M1DEA in this specific combination.

Further, we can estimate a mean impact expected in region A due to any variation of the Earth structure in region B, which is then simply the mean of all tested "specific impacts" (Eq. (4)):

$$\overline{\Delta\psi} = \frac{1}{N_{\mathrm{mod}}} \sum_{v,w} |\psi_{B,v} - \psi_{B,w}| \tag{5}$$

N_{mod} is then the number of combinations of Earth structures v and w. Both, specific and mean impact, are given in absolute values of displacement rates and of course have to be interpreted locally with respect to the predicted rates $\psi(\vartheta, \varphi)$ at that point.

4. Results

Both SLC and GIA uplift rates contain an elastic contribution from present loading and a viscous contribution from past loading. Here, we show the sensitivity of these contributions to variations of the Earth structure – exemplary for the uplift rates and GIA modeling.

4.1. Impact on the elastic contribution

We test the sensitivity of the elastic contribution by studying the elastic response to uniform present-day Antarctic ice loss (WANT$_{el}$). In the pseudo-spectral SLE the elastic contribution is affected only by thickness, density, and shear modulus of the EL. In our setup only EL thickness variations affect the elastic contribution, since density and shear modulus are changed implicitly using the PREM average within each layer. However, even the largest EL variation in our test range (40 km vs. 120 km) causes at most only $|\Delta u| < 5$ µm directly along the margins of the ice load (Fig. 4). Everywhere else this effect is even smaller such that $|\Delta u| \ll 1$ µm. This is $\ll 1\%$ of the eustatic rate of WANT$_{el}$. Thus, the impact of EL variations – in a reliable range – on uplift rates induced by WANT$_{el}$ can be seen as neglectable.

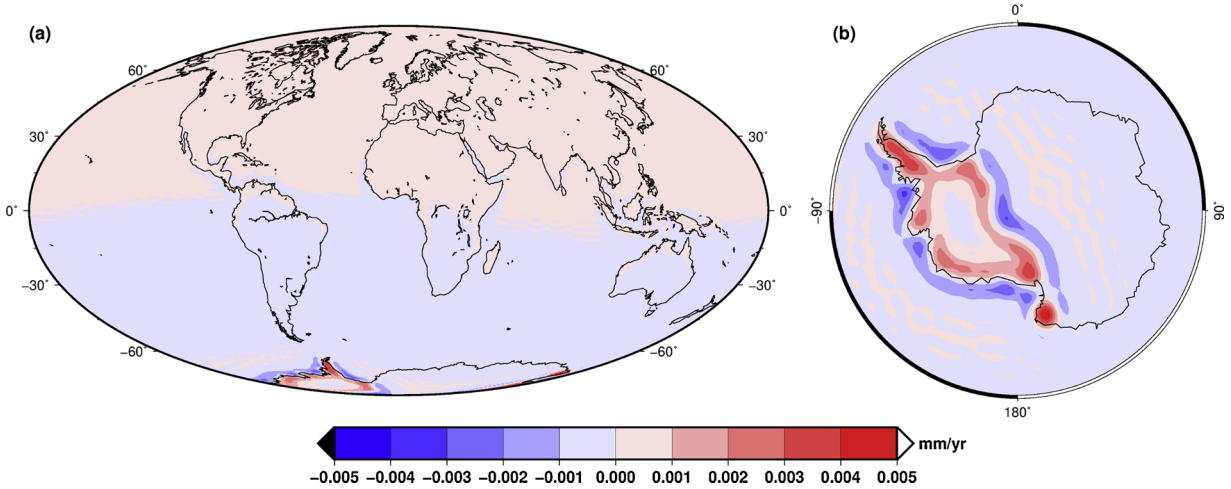

Fig. 4. Difference of the elastic uplift rate from the present-day loading scenario WANT$_{el}$ between an elastic lithosphere of $d_{EL} = 120$ km and $d_{EL} = 40$ km. (The colored figure is available in the web version of this article.)

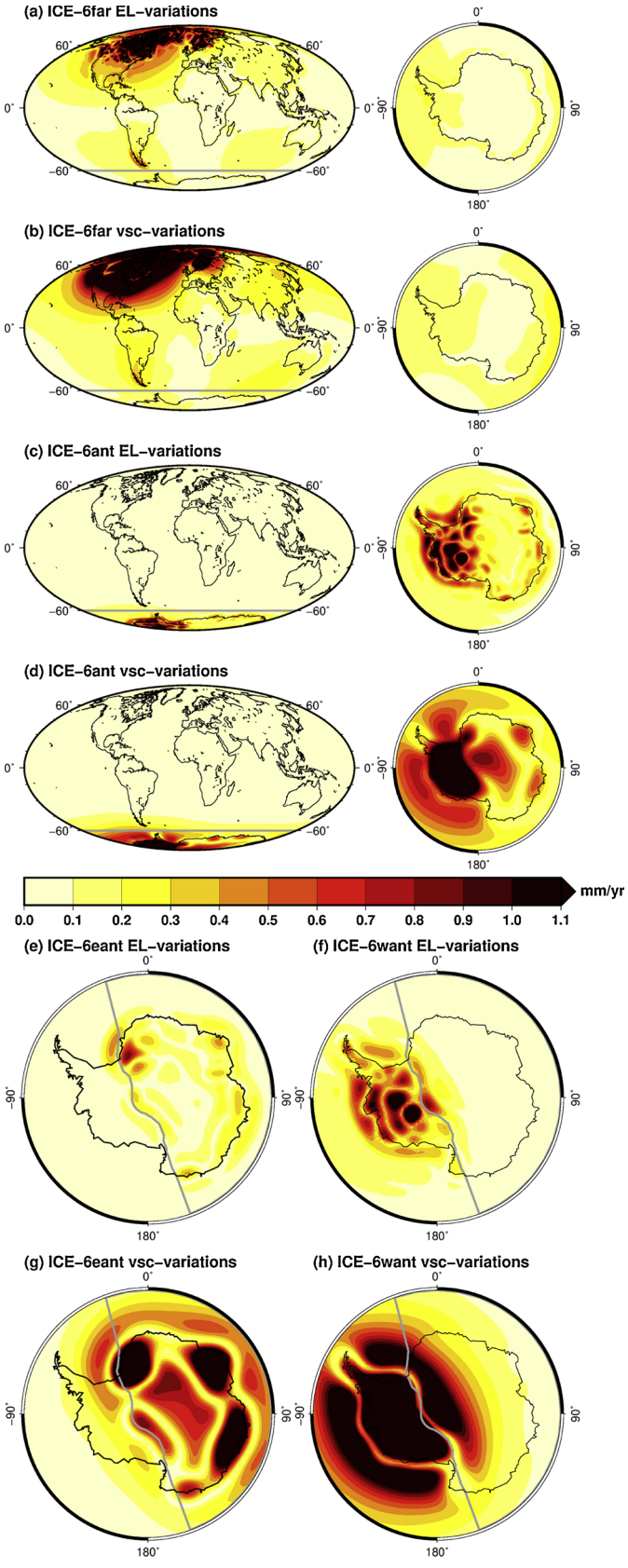

Fig. 5. Mean impact $\overline{\Delta u}$ (Eq. (5)) of Earth structure variations on present-day GIA uplift rates, for the different components of the ICE-6G loading scenario. The variations shown here should be compared to uplift rates of $u \approx 5\,\frac{\text{mm}}{\text{yr}}$, which are typical of GIA processes.
Top: Mean impact for far-distant variations. (a) EL variations for ICE-6far, (b) viscosity variations for ICE-6far, (c) EL variations for ICE-6ant, (d) viscosity variations for ICE-6ant. The mean impact in (a),(c) comprises $N_{\text{mod}} = 96$ model combinations using an EL variation of $d_{\text{EL}} = 120$ km to $d_{\text{EL}} = 40$ km with non-varying viscosities $\mu_{\text{SUM,DUM,TZ}}$. The mean impact in (b),(d) comprises $N_{\text{mod}} = 1269$ model combinations using a constant EL thickness of $d_{\text{EL}} = 120$ km with combinatorial varying viscosities $\mu_{\text{SUM,DUM,TZ}}$ within the test range between local and far-field Earth structure. The gray line in (a)–(d) marks the separation of Antarctic and Non-Antarctic regions.
Bottom: Mean impact of near-distant variations. (e) EL variations for ICE-6eant. (f) EL variations for ICE-6want. The mean impact in (e),(f) comprises $N_{\text{mod}} = 96$ model combinations using an EL variation of $d_{\text{EL}} = 120$ km to $d_{\text{EL}} = 60$ km with non-varying viscosities $\mu_{\text{SUM,DUM,TZ}}$. (g) viscosity variations for ICE-6eant. (h) viscosity variations for ICE-6want. The mean impact in (g),(h) comprises $N_{\text{mod}} = 47$ model combinations using a constant EL thickness of $d_{\text{EL}} = 120$ km, the $\text{W12}_{\text{earth}}$ for East Antarctica and varying viscosities $\mu_{\text{SUM,DUM,TZ}}$ within the test range for the West Antarctica Earth structure. The gray line in (e)–(h) marks the separation of the East and West Antarctic regions. (For interpretation of the references to color in the text, the reader is referred to the web version of this article.)

4.2. Impact on the viscous contribution

We test the sensitivity of the viscous contribution by examining the GIA response to the long-term ice loading scenario ICE-6G. Generally, the viscous contribution is affected by both EL variations and viscosity variations. We found that Earth structure variations at great distances show a neglectable mean impact (Eq. (5)) on the local uplift rates for both types of variations. We compute the mean impact of the EL variations (Fig. 5(a),(c)) from the 96 model combinations with the largest EL variation within our test range ($d_{\text{EL}} = 120$ km vs. $d_{\text{EL}} = 40$ km) in combination with non-varying viscosities $\mu_{\text{SUM,DUM,TZ}}$.

The mean impact of the viscosity variations (Fig. 5(b),(d)) involves the 1269 model combinations with varying viscosities between the Antarctic and Non-Antarctic Earth structure based on all 48 viscosity settings in the Antarctic region and 27 settings in the Non-Antarctic region (excl. $\mu_{\text{SUM,DUM}} = 10^{18}$ Pa s). The EL thickness in both Earth structures is held at $d_{\text{EL}} = 120$ km. Both load components (ICE-6far, ICE-6ant) show a large mean impact $\overline{\Delta u} > 0.6\,\frac{\text{mm}}{\text{yr}}$ in their local region around their characteristic distribution of the ice load (Fig. 5(a)–(d), red/black areas), where we account for the variations, but only a minor impact of $\overline{\Delta u} < 0.2\,\frac{\text{mm}}{\text{yr}}$ (white/yellow areas) in their far-field region. These mean impacts on uplift rate should be compared to uplift rates of $u \sim 5\,\frac{\text{mm}}{\text{yr}}$, which is a typical value for the main pattern of uplift in Antarctica from the ICE-6G(VM5a) loading scenario (Argus et al., 2014).

We analyzed in the same manner the mean impact of variations at near distances via the load components ICE-6eant and ICE-6want (Fig. 5(e)–(h)). For EL variations, we computed the mean impact of 96 model combinations of non-varying viscosities, but with an EL variation of $d_{\text{EL}} = 120$ km vs. $d_{\text{EL}} = 60$ km (Fig. 5(e),(f)). Again the EL variations exert a negligible impact on the uplift rates of the neighboring region. For viscosity variations, the mean impact is based on the assumption of a stiff East Antarctic Earth structure. We assume the East Antarctic Earth structure to follow $\text{W12}_{\text{earth}}$. Thus the mean impact involves the 47 model combinations with differing viscosities and an EL thickness of $d_{\text{EL}} = 120$ km (Fig. 5(g),(h)). The viscosity variations show a much larger mean impact in the neighboring regions. Especially variations beneath West Antarctica, which affect the response to ICE-6want, can

have a significant influence in large areas of East Antarctica (Fig. 5(h)). However, these results (Fig. 5) are based only on the long-term loading of ICE-6G. Next, we demonstrate how this impact in neighboring regions can decrease if the considered time period of loading matches the relaxation behavior of the Earth structure.

4.3. Influence of the time period of loading

Here, we apply the M1DEA to consider the different Earth structures beneath East and West Antarctica. East Antarctica uses the stiff Earth structure ($W12_{earth}$, blue line in Fig. 2) while West Antarctica uses the low-viscosity estimate (BAR_{earth}, red line in Fig. 2). The present-day uplift rates from only long-term loads (Fig. 6(a)) show large amplitudes in East Antarctica, where the GIA is still ongoing due to the slow relaxation of the rigid Earth structure. The uplift rates in West Antarctica are drastically smaller, since the faster relaxation of the less viscous Earth causes a nearly finalized GIA. On one hand the impact of the more rigid East Antarctic Earth structure on the West Antarctic uplift rates (Eq. (4)) results from the "unexpected" slow relaxation of East Antarctica, but is mostly limited to the margins along the transition of both load components (Fig. 6(b)). On the other hand the "missing" long-term load signal of the fast relaxing West Antarctica causes the large impact on neighboring stiff regions (Fig. 6(c)).

In the case of a fast relaxing low-viscosity Earth structure, recent deglaciation is the major contribution to the present-day uplift rates, as observed if $WANT_{100}$ is included additionally to the loading scenario (Fig. 6(d)). This leads to an enormous reduction in the differences induced by the less viscous West Antarctic structure (Fig. 6(f)). The differences mainly follow variations in the spatial distribution of West Antarctic ice loss between the long-term and recent loads. The only strong anomaly remaining as impact on the East Antarctic uplift rates is a tiny belt of subsidence from the collapsing bulges around the recent load (Fig. 6(f)).

Alternatively, the W12 ice loading scenario (Whitehouse et al., 2012a,b) can be used as a long-term model. Using W12 loading confirms the results using ICE-6G (Figs. 5 and 6), resulting in similar mean impacts and even smaller differences when the recent load is included (see Appendix B: Figs. B.2 and B.3).

5. Assessment of the M1DEA

The existing global predictions of SLC and GIA (e.g., ICE-6G(VM5a), Peltier et al., 2015), which are based on a classical radially-symmetric Earth structure, are not able to explain regionally-observed rapid uplift rates, e.g., in the Amundsen Sea Embayment (Barletta et al., 2018). The presented M1DEA and recent similar approaches (Khan et al., 2016; Sasgen et al., 2017, 2018) can implement a locally-appropriate Earth structure and therefore allow us to consider lateral variations in Earth structure. As our sensitivity analysis of the M1DEA (Fig. 5) reveals, a considered variation of the Earth structure for a specific load component affects mainly the region of the load component itself and a relatively narrow region surrounding it. For an ice history involving both long-term and recent loading, the M1DEA improves estimates of SLC and GIA in regions with strong viscosity variations compared to using a single 1D Earth structure. According to the analysis of Paulson et al. (2005), displacement rates are strongly sensitive to the local viscosity structure beneath the load and observation point, and less related to the global mean structure. This supports the application of the M1DEA to account for viscosity anomalies below the different load components, although the M1DEA cannot consider potential viscosity anomalies for

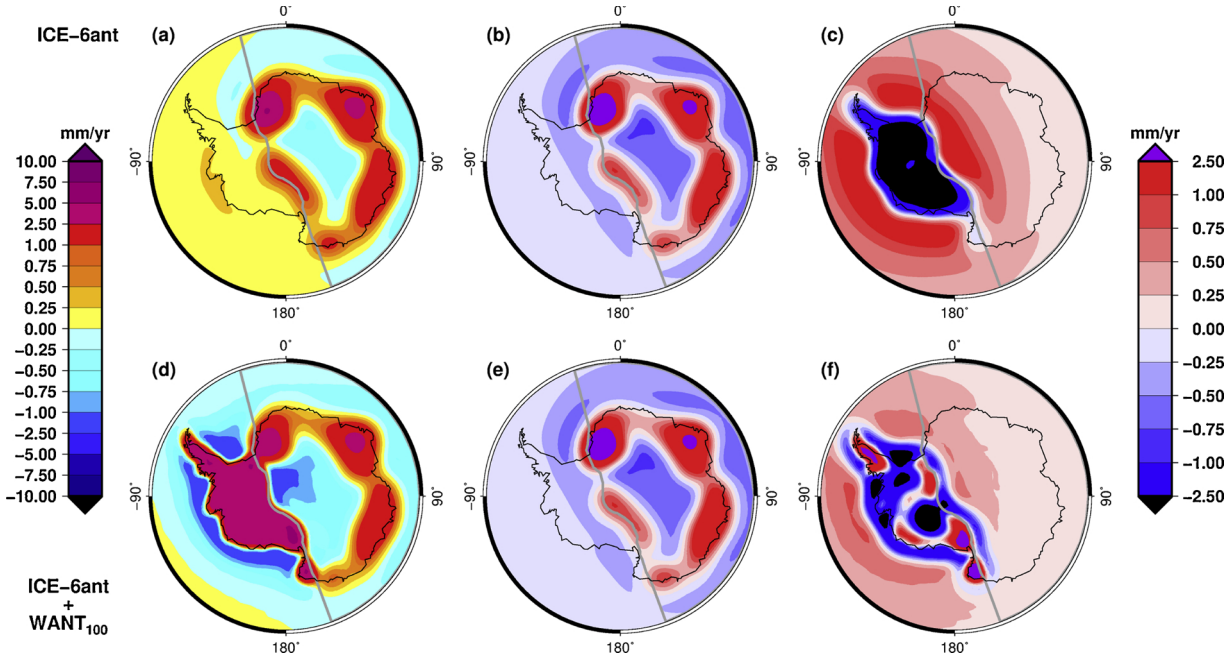

Fig. 6. M1DEA applied for Antarctic deglaciation using a strong lateral contrast (rigid East Antarctic structure $W12_{earth}$, and super low-viscosity West Antarctic structure BAR_{earth}, see Table A.3, Fig. 2).
Top row: Using only long-term loads of ICE-6G components: (a) Combined uplift rates, (b) Differences Δu (Eq. (4)) between the combined and homogeneous uplift rates of the low-viscosity Earth structure, (c) Differences Δu between the combined and homogeneous uplift rates of the rigid Earth structure.
Bottom row: Using long-term loads of ICE-6G components and recent load ($WANT_{100}$): (d) Combined uplift rates, (e) Differences Δu between the combined and homogeneous uplift rates of the low-viscosity Earth structure, (f) Differences Δu between the combined and homogeneous uplift rates of the rigid Earth structure. The gray line marks the separation of East and West Antarctica. (The colored figure is available in the web version of this article.)

the observation points. Such a treatment requires a fully 3D finite element model (Paulson et al., 2005).

Nevertheless, the M1DEA represents a straight-forward approximation to test the effect of lateral variations in Earth structure. In particular, the combined rates of the M1DEA result from multiple definitions of a globally uniform relaxation behavior. Thus, they contain contributions from the various different load components, each modeled with a different and locally-appropriate Earth structure. By contrast, the globally uniform relaxation behavior of a 1D Earth structure implies spatially symmetric transmission of stresses and flow patterns around any load. Using only a single 1D Earth structure, the equal relaxation behavior compensates the influence of neighboring load components. The superposition of uplift and SLC rates from different uniform relaxation behaviors interrupts this implicit compensation between neighboring regions.

Compared to full 3D finite element/volume solutions any asymmetric transmission of stresses at the margins of the neighboring components is neglected by the M1DEA (Khan et al., 2016; Sasgen et al., 2018). The differences between a full 3D model and M1DEA solutions are thus expected to be largest along the margins of neighboring regions with different Earth structures. In particular, peripheral bulges within the M1DEA are predicted from the Earth structure beneath the corresponding load component, even if the bulge might be located in a neighboring region with a different Earth structure (Fig. 7). Our sensitivity analysis (Fig. 5(e)–(h)) clearly reveals this bulge impact in the neighboring region, and illustrates what may be the largest source of modeling error associated with the M1DEA. However, our results for Antarctica are consistent with the recent comparison of a 3D vs. 1D Earth structure by Hay et al. (2017), who used a finite volume model.

In the following we discuss the impact of this cross-region effect for the different parameters of the Earth structure and different aspects of M1DEA solutions, and how it can be minimized.

5.1. Modeling variations in elastic lithosphere

In general, the influence of the EL thickness on present-day uplift rates becomes apparent in small-scale variations of the viscous (post-glacial) response. These variations mainly affect the short wavelength patterns of uplift rates related to small-scale structures of the chosen loading scenario. A thinner EL increases the amplitudes and shortens the wavelength of the predicted uplift rates, compared to the thicker EL. This behavior is also demonstrated by the 3D approach of Nield et al. (2018). The mean impact $\overline{\Delta u}$ (Eq. (5)) from EL variations is strongly limited to each region and shows only neglectable effects on other regions (far-distant and near-distant, Fig. 5(a),(c),(e),(f)). This indicates reasonable results for the M1DEA when considering EL variations in the predictions of viscous uplift rates, despite the neglected asymmetric transmission of stresses.

The elastic response of the Earth shows a neglectable sensitivity to strong variations of the EL thickness (Fig. 4). Consequently, no significant accuracy is gained, but also no bias is introduced, by the M1DEA in the predicted elastic contribution. This enhances the findings of Mitrovica et al. (2011), and confirms the typical fingerprint character of the elastic contribution mainly determined by the location and amount of (ice or water) load.

5.2. Modeling variations in upper mantle viscosities

Laterally-varying upper mantle viscosities affect the entire large-scale uplift pattern including both the region of ice loading and the surrounding bulges in the near-field of the local ice load. Hence, the mean impact $\overline{\Delta u}$ (Eq. (5)) of viscosity variations beneath near-distant and neighboring loads shows a potentially large influence on the local rates (Fig. 5(g),(h)), whereas the effect of a viscosity variation beneath a far-distant load remains locally still neglectable (Fig. 5(b),(d)).

Strong contrasts of the upper mantle viscosities between

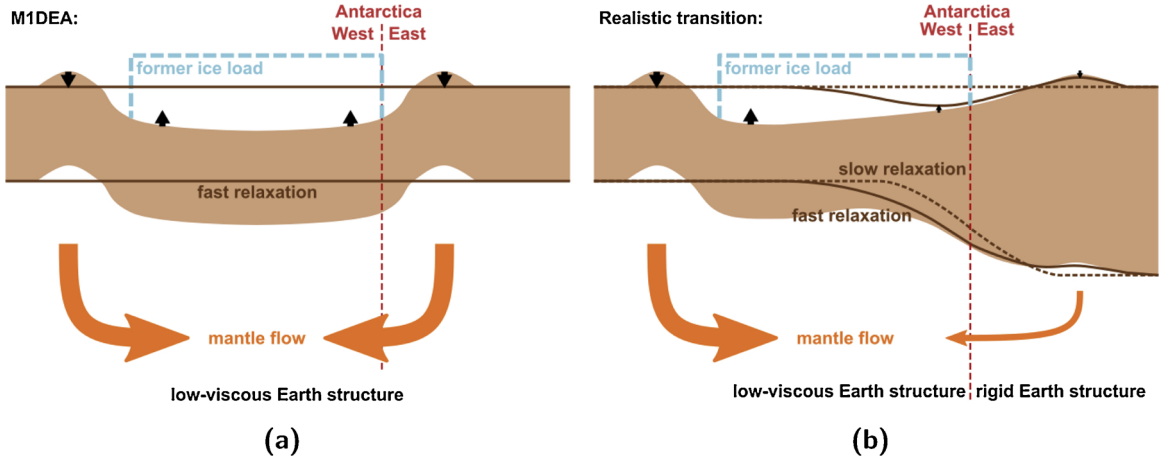

Fig. 7. Schematic GIA effect for a load (dashed blue) on a low-viscosity Earth structure (like West Antarctica) in the direct vicinity of a transition to a high-viscosity Earth structure (like East Antarctica). The red dashed line marks the border between both regions. The brown area is the initial state of the EL. The solid brown lines mark the state after the full relaxation of the low-viscosity structure. The dashed brown lines show the state after the full relaxation of the high-viscosity structure. The orange arrows indicate the mantle flow, and the black arrows the observed uplift rates during the fast relaxation. (a) The predicted relaxation by the M1DEA assumes a globally West Antarctic structure with a laterally-symmetric relaxation. As the entire load is located on the low-viscosity structure, the bulge in East Antarctica still follows the fast relaxation. The GIA is already finalized after the fast relaxation (solid brown = dashed brown). (b) The relaxation of a realistic transition introduces an asymmetric initial deformation. The low-viscosity side fully relaxes in the first phase with large mantle flow and large uplift rates. The high-viscosity side is characterized by a different initial deformation of longer wavelength and smaller amplitude, and relaxes only slowly with less mantle flow and small uplift rates during the first period of faster relaxation. (For interpretation of the references to color in this figure legend, the reader is referred to the web version of this article.)

neighboring regions cause large differences in their time scales of relaxation. High viscosities lead to a slow relaxation with present-day rates most sensitive to ice loading at 1 to 100 kyr before present, whereas low viscosities result in a much faster relaxation, with the highest amplification resulting from ice loading that happened decades or centuries ago. For the M1DEA, this results in two magnifying effects: First, the stronger contrasts result in larger differences in rates between regions due to inhomogeneous compensation of bulges from connected loads. Second, the fast relaxation for low-viscosity Earth structures can diminish the local contribution to the rates obtained from long-term loading scenarios (Fig. 6(a)). Both yield large impacts Δu (Eq. (4)) on local uplift rates along the margins of neighboring load components with strong viscosity contrasts between them (Fig. 6(a)–(c)), according to the general discussion above.

We clearly demonstrate that the inclusion of a recent ice load in a region of fast relaxation can drastically reduce the specific impact Δu (Eq. (4)) of the low-viscosity region on neighboring regions (Fig. 6(d)–(f)), in particular if recent and long-term loading act in parallel (e.g., ice loss for both). The recent ice loss introduces an additional contribution, which recovers the dominance of the contribution from the local load component in the local rates (compare the West Antarctic region in Fig. 6(d) vs. (a)). Further, the rapid response to the recent ice loss compensates the missing counterpart of the peripheral bulge at the margins of neighboring deglaciating regions, which mimics to some degree the behavior of a 3D Earth structure as observed in Hay et al. (2017). Depending on the recent ice change, this effect will be largest for strong contrasts that include very low viscosities. How accurately this synthetic combination embodies the actual 3D effects at the margins cannot be explicitly clarified in this paper and must be tested against a full 3D finite element approach using various lateral Earth structure variations for a range of grid resolutions and maximum spherical degrees, respectively.

Any type of modeling that includes lateral variations of upper mantle viscosities requires regional components that deglaciate at the time scales of their regional relaxation. Thus, the M1DEA provides a computationally cheap way to assess the effect of even strong lateral variations of upper mantle viscosity between large-scale load components.

5.3. Modeling with large-scale and small-scale components

Assuming the same arbitrary Earth structure, a large-scale load is associated with stronger bulges of longer wavelength than a small-scale load. Consequently, large-scale loads have a bigger bulge impact Δu (Eq. (4)) on the rates in the neighboring region. Also, a strong contrast in the Earth structure between neighboring load components leads to a broader bulge impact along the Earth structure variation. Introducing more small-scale components in the vicinity of a strongly varying Earth structure (e.g., the Trans Antarctic mountains) allows M1DEA to address variations in Earth structure more continuously with smaller contrasts. This should significantly reduce the big bulge impacts in such regions, since:

- The smaller contrasts may introduce bulges that better compensate each other, like uniform structures would do.
- Smaller scale load components affect narrower margins along the transition.

The tests in this paper are based on large-scale components with relatively strong contrasts between their Earth structures and do not include a small-scale load transition. Therefore, the obtained differences should define an upper limit for the amplitude and wavelength of the bulge impact of the neighboring Earth structure along the margin. Nevertheless, these models already show differences, which justify the application of the M1DEA. Thus with the addition of a small-scale load transition, the M1DEA would seem to offer great capabilities to model GIA and SLC for lateral variations in Earth structure for relatively small computational cost. Recent GIA models for Greenland (Khan et al., 2016) and Antarctica (Sasgen et al., 2017, 2018) have already started to use the M1DEA with small-scale components. However, it cannot completely be ruled out that very large contrasts on a small scale within the 3D Earth structure may compromise the accuracy of the M1DEA. Here as well, further tests against fully 3D finite element models are needed to investigate the accuracy of the M1DEA along the transition between neighboring Earth structures for continuous variations with small-scale load components. These tests should consider many parameters for both approaches, e.g., the grid resolution of the finite element model, the maximum spherical harmonic degree of the M1DEA, the number and size of load components in the M1DEA, in order to compare both approaches in accuracy and computation time.

5.4. Modeling rotational feedback

Above we discussed the possible local artifacts of the M1DEA that are directly linked to the margins of neighboring load components. These are of course the most obvious uncertainties. Beside these local effects, SLC and GIA also include global features that are mainly decoupled from the load location, e.g., the RFB. The RFB always appears with a spherical harmonic (2,1)-pattern varying in amplitude depending on load amount, load position, loading time, and the Earth structure. The M1DEA simply combines classical 1D SLE solutions for multiple load components with global 1D Earth structures, which are locally-appropriate (Eq. (3)). Thus, the RFB contribution of each solution assumes the locally-appropriate Earth structure to be globally valid. Consequently, we cannot rule out that including RFB within the M1DEA might over- or underestimate the RFB contribution of some load components compared to the real 3D rheology structure of the entire Earth, which can affect coupling to other harmonics on a self-gravitationally consistent Earth (Paulson et al., 2005).

To deal with this problem following the idea of the M1DEA, we suggest that either an estimate of the total RFB by a mean Earth structure (i.e., less M1DEA) or a separate modeling of the ocean load of each component with a consistent oceanic Earth structure (i.e., even more M1DEA!) can reduce this uncertainty and increase the accuracy of the estimated total RFB. However, our calculations show that the Antarctic load components induce too little viscous RFB - most probably due to their location too close to the South pole – to satisfy a detailed analysis of the RFB approximation within the M1DEA that would be comparable to the treatment by Paulson et al. (2005).

6. Conclusions

We tested a new approach for using the pseudo-spectral form of the sea level equation (SLE) to account for lateral variations in Earth structure, namely upper mantle viscosities and elastic thickness of the lithosphere. This Multiple 1D Earth Approach (M1DEA) predicts global sea level change (SLC) and ground uplift rates using the superposition of separately calculated solutions of the pseudo-spectral SLE for each regional component of the ice load. Lateral heterogeneity in Earth structure is accommodated in M1DEA by utilizing different, locally-appropriate, 1D Earth structures for each individual solution. Our analysis of the sensitivity of local uplift rates to variations in Earth structure suggests:

1. The elastic contribution of SLC and uplift rates is (nearly) independent from Earth structure variations. Therefore, the M1DEA is applicable without any bias, but also without much benefit, for the predictions of elastic sea level fingerprints.

2. The viscous contribution is strongly affected by Earth structure variations. However, the effect of variations in elastic thickness of the lithosphere is locally limited, meaning that the M1DEA can usefully account for such variations.
3. The viscous contribution to SLC and uplift rates depends on the local viscosity structure but also to some degree on the viscous structure of neighboring regions. This inability to adequately handle peripheral bulges that extend into neighboring regions with differing viscosity structures is a limitation of the M1DEA. However, the M1DEA can account for viscosity variations if:
   (a) Each regional load component includes deglaciation associated with its individual time scale of relaxation, i.e., short-timescale loads are present in fast-relaxing regions (such as West Antarctica), and longer-timescale loads are present in more slowly relaxing regions (such as East Antarctica).
   (b) The load is subdivided into small-scale components in areas of strong variations, in order to maintain small viscosity contrasts between neighboring Earth structures.

In summary, our sensitivity analysis of the M1DEA for the pseudo-spectral SLE demonstrates the potential in its application. Further tests should compare predictions from M1DEA models directly against 3D finite element models (3D FEM) to characterize the relative accuracy of the M1DEA (in particular regarding recommendation 3.b), and its benefit in terms of computation time, with respect to the grid resolution (3D FEM), the maximum spherical harmonic degree (M1DEA), and the number of load components (M1DEA). A sophisticated M1DEA can potentially contribute usefully to more accurate predictions of GIA-inferred uplift rates at reduced computational cost. Such predictions are essential for enhancing models of Antarctic ice history, estimates of recently accelerated present-day Antarctic ice loss, and the probability of a future collapse or stability of Antarctic ice sheets. In the future, coupled climate models will hopefully benefit from these improvements.

Conflicts of interest

The authors declare no conflicts of interest.

Acknowledgments

We thank the editor, Irina Artemieva, and two anonymous reviewers for their critical feedback, which helped to improve the manuscript. Furthermore, we thank Pippa Whitehouse for her kind cooperation in providing her ice model and the following discussion, which clarified issues related to ESL and the important difference between total and effective ice thickness. This work was supported partly by the Research Council of Norway's projects 223272 (Centre of Excellence) and 288449 (CPC).

Appendix A. Data and setup details

The effective ice load $I_i(\vartheta, \varphi)$ at each location (ϑ, φ) and time step i, i.e., the ice above neutral buoyancy, is estimated from the original total ice thickness $I_{i,\mathrm{tot}}(\vartheta, \varphi)$ using the present-day bathymetry $Z(\vartheta, \varphi)$ (Fig. A.1) via:

$$I_i(\vartheta, \varphi) = \begin{cases} I_{i,\mathrm{tot}}(\vartheta, \varphi) & : Z(\vartheta, \varphi) > 0 \\ I_{i,\mathrm{tot}}(\vartheta, \varphi) + \frac{\rho_w}{\rho_{ice}} Z(\vartheta, \varphi) & : Z(\vartheta, \varphi) < 0,\ I_{i,\mathrm{tot}}(\vartheta, \varphi) > |\frac{\rho_w}{\rho_{ice}} Z(\vartheta, \varphi)| \\ 0 & : Z(\vartheta, \varphi) < 0,\ I_{i,\mathrm{tot}}(\vartheta, \varphi) \leq |\frac{\rho_w}{\rho_{ice}} Z(\vartheta, \varphi)| \end{cases} \quad \text{(A.1)}$$

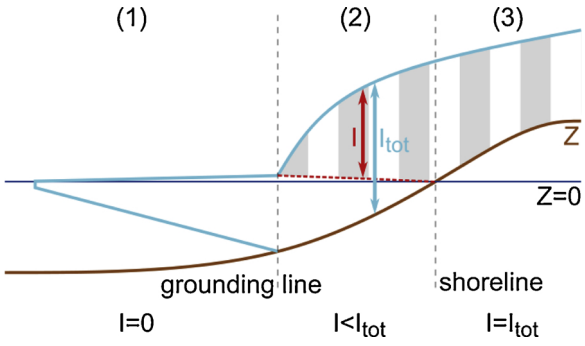

Fig. A.1. Schematic illustration of effective loading thickness and total thickness of ice sheets: (1) Marine ice swims completely in buoyancy and will neither change the effective load, nor the ESL, when it melts. (2) Marine-grounded ice is partly in buoyancy and affects the local effective load and ESL only above $I_{i,\mathrm{tot}}(\vartheta, \varphi) = |\frac{\rho_w}{\rho_{ice}} Z(\vartheta, \varphi)|$. (3) Onshore grounded ice contributes completely to loading and ESL. (The colored figure is available in the web version of this article.)

Table A.1
Numerical setup of *SELEN* used for all calculations of the SLE in this publication.

Parameter	Description	Value
l_{max}	Max. spherical harmonic degree	128
N_{it}	Number of iterations	3
R	Grid resolution parameter	44
N_p	Number of global pixels	75,692
	Degree $l = 1$ Love numbers	Included
	Reference frame	Center of mass

Table A.2
Summary of the layers and their general parameters for all Earth structures in this publication. The star * indicates values that are PREM-averaged within the different layers. Hence, the density and shear moduli of EL and SUM depend on the chosen thickness $d_{EL} \in [40\,\text{km}, 120\,\text{km}]$, but are still PREM averaged. 'var' marks an arbitrary variable.

Layer	Basal depth d [km]	Density $\rho\left[\frac{\text{kg}}{\text{m}^3}\right]$	Shear modulus G [10^{11} Pa]	Viscosity μ
EL	[40, 120]	*	*	elastic
SUM	220	*	*	var
DUM	400	3475.5*	0.7649*	var
TZ	670	3857.7*	1.0648*	var
LM	2891	4877.9*	2.1948*	var
Core	6371	10931.7*	0	0

Table A.3
Summary of the variable parameters for the Earth structures in this publication: d_{EL} is the thickness of the EL. $\mu_{SUM,DUM,TZ,LM}$ are the viscosities in the four mantle layers SUM, DUM, TZ, and LM. Within the test range the parameters can be any of the distinct multiple values for each layer. All structures use a lower mantle viscosity of $\mu_{LM} = 10^{21.5}$ Pa s.

Structure	d_{EL}	μ_{SUM}	μ_{DUM}	μ_{TZ}	μ_{LM}
	[km]	[$\log_{10}$ Pa s]			
$W12_{earth}$	120	21	21	21	21.5
BAR_{earth}	60	18.6	19.2	19.4	21.5
Test range	{40, 60, 90, 120}	{18, 19, 20, 21}	{18, 19, 20, 21}	{19, 20, 21}	21.5

Table A.4
Ice loading scenarios used in this publication and their characteristic parameters: The ESL contribution refers to the change after the LGM until now. The temporal discretization $\Delta t_{Deglac,Glac}$ for the deglaciation/glaciation period considers ice changes after/before the LGM. The spatial grid resolution $\Delta\vartheta$ and $\Delta\varphi$ is uniform in longitudinal and latitudinal direction. The selected bathymetry data set is used for the approximation of the effective ice load of the original ICE-6G files (http://www.atmosp.physics.utoronto.ca/~peltier/data.php, downloaded 06.06.2018).

Component	ESL [m]	Δt_{Deglac} [kyr]	Δt_{Glac} [kyr]	$\Delta\vartheta$, $\Delta\varphi$	Bathymetry
ICE-6far	113.86				ETOPO
ICE-6ant	11.69				BEDMAP2
ICE-6eant	3.88	0.5	2.0	1°	BEDMAP2
ICE-6want	7.81				BEDMAP2
$WANT_{el}$	$4.6\,10^{-4}$	0.001	–	0.5°	–
$WANT_{100}$	$4.6\,10^{-2}$	0.01	–	0.5°	–

Appendix B. Supporting results

To Fig. B.1: In previous tests we have analyzed the uplift rates in the Antarctic region and outside Antarctica. These tests motivated the M1DEA and the sensitivity analysis presented in this paper.

In these tests we solved the SLE for each load component (ICE-6far, ICE-6ant, W12) for all 192 Earth structures. The difference between the rotating and the non-rotating solutions yields the RFB contribution for each combination of load component and Earth structure. For comparison, we calculated the L_2-norm of uplift rates within the region Reg: $||\vec{u}_{\text{Reg}}||_2 = \sqrt{\sum_p u_p^2}, \quad \forall\, p \in \text{Reg}$, where the rates u_p are computed at pixels p within the region Reg. Gathering the values of this regional L_2-norm depending on the observed region, the applied load component, and the non-rotating and RFB contributions, yields 12 distributions of L_2-norms each with a sample size of $N = 192$ (Fig. B.1).

It can be observed that uplift rates are dominated by their local component of ice loss – (nearly) independently of the Earth structure (Fig. B.1(a) 1st panel, (b) 2nd panel). This supports our initial assumption for the M1DEA (Fig. 1). Furthermore, Antarctic long-term ice loss is not able to induce a significant RFB contribution to the total rates in any component on a postglacial time scale ($\approx$1%) (Fig. B.1 4th panel).

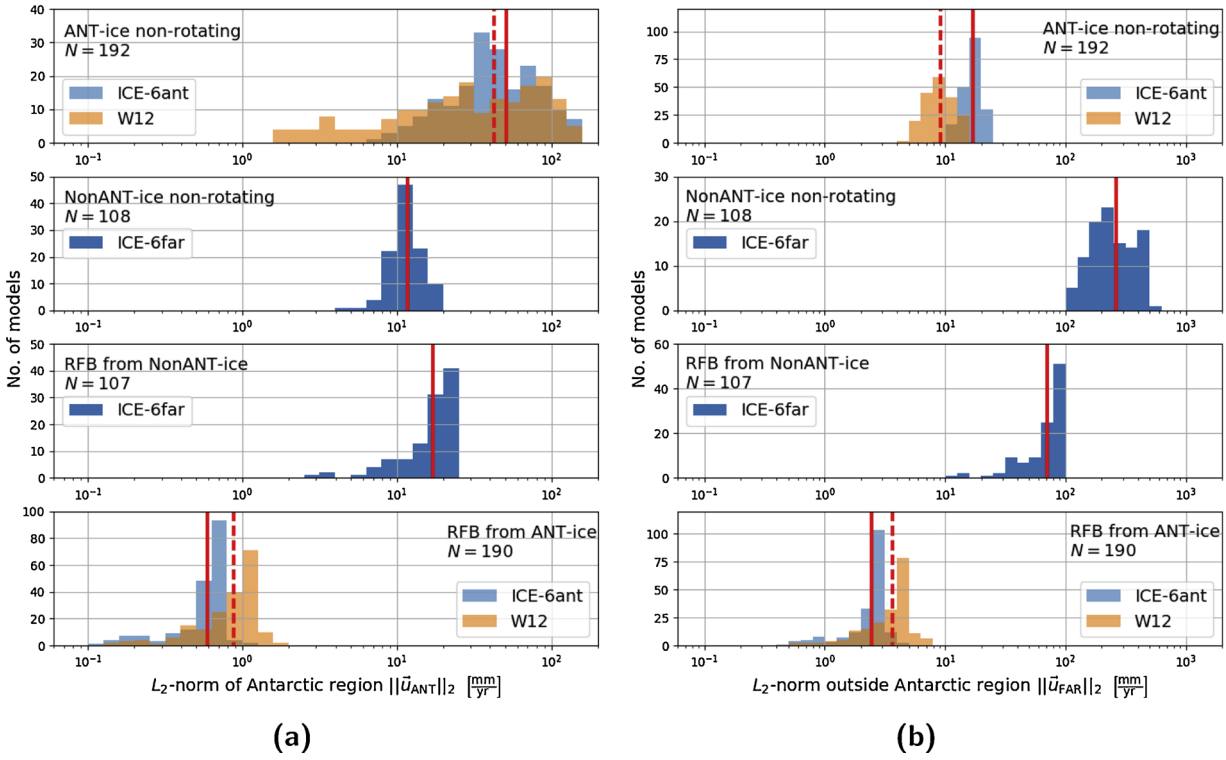

Fig. B.1. Regional average uplift rates in (a) the Antarctic region (south of 60°*S*), and (b) the Non-Antarctic region (north of 60°*S*). Each panel shows the distribution of the regional average uplift rate for the 192 tested Earth structures for a specific load contribution. The four panels from top to bottom show the contributions from the Antarctic ice load on a non-rotating Earth, the Non-Antarctic ice load on a non-rotating Earth, the RFB induced by the Non-Antarctic ice load, and the RFB induced by the Antarctic ice load. Each value in the different distributions represents the regional L_2-norm of uplift rates of one load-Earth-combination. The red lines mark the mean values of the distributions for each contributor (red solid: ICE-6 components, red dashed: W12 component). (For interpretation of the references to color in this figure legend, the reader is referred to the web version of this article.)

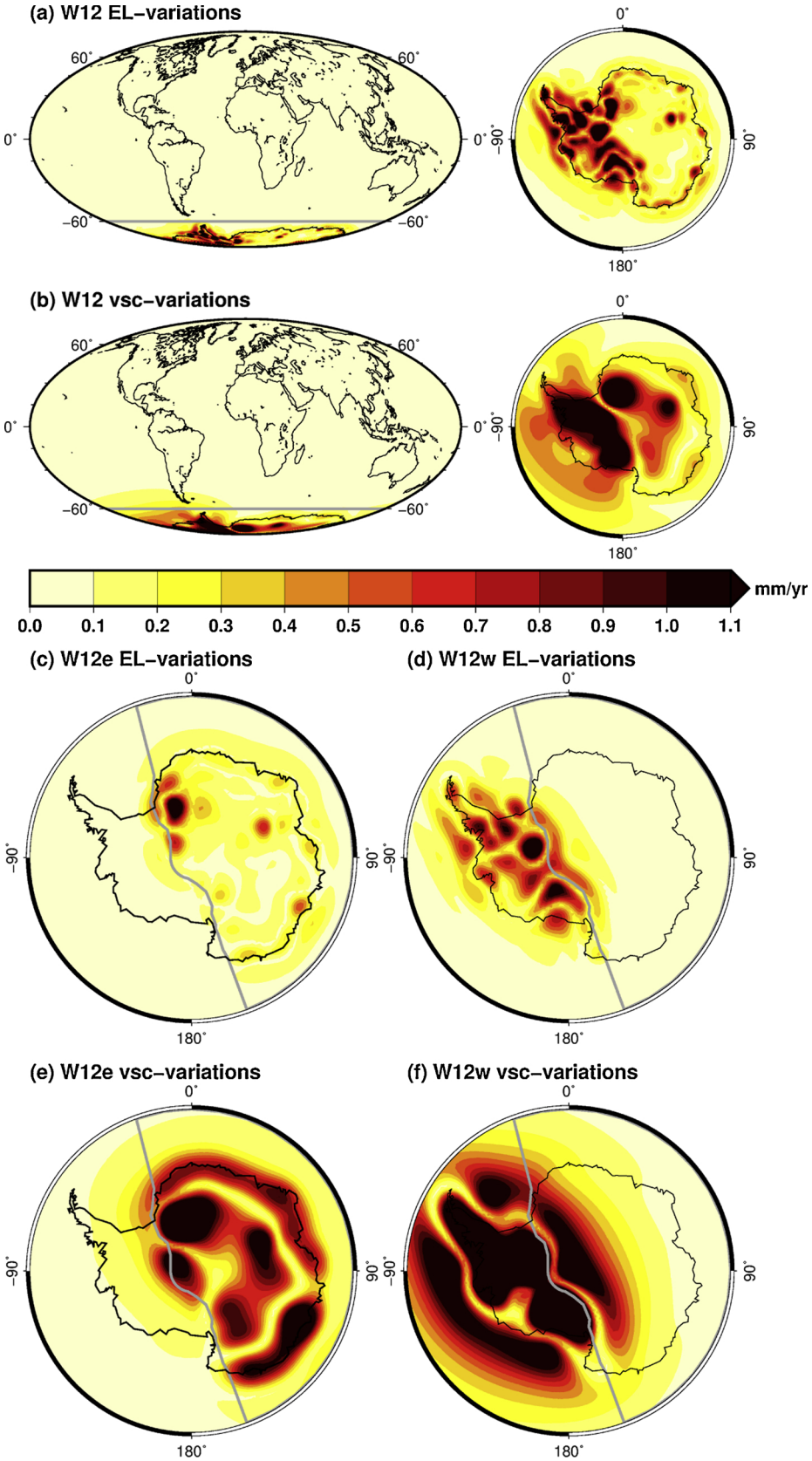

Fig. B.2. Mean impact $\overline{\Delta u}$ (Eq. (5)) of Earth structure variations on present-day GIA uplift rates, for the different components of the W12 loading scenario. See Fig. 5, which shows the same analysis for the ICE-6G loading scenario, for an explanation of the figure. (The colored figure is available in the web version of this article.)

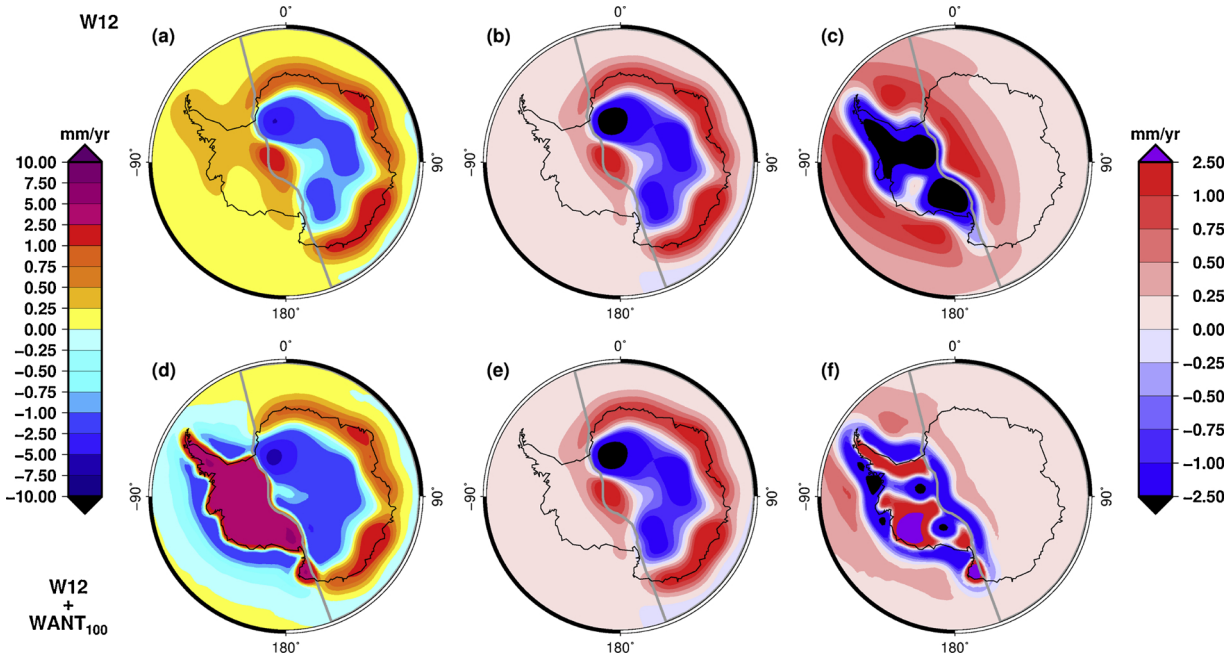

Fig. B.3. Similar to Fig. 6 of the main text, but using W12 ice loads instead of ICE-6G. (The colored figure is available in the web version of this article.)

Appendix C. Implementation of rotational feedback in *SELEN*

The repository https://github.com/r-hartmann/RFBupdate_for_SELEN/ provides:

- All subprograms (modified and new) that are required to include the RFB option in *SELEN* 2.9.12
- An installation guide
- Implementation details
- Theoretical background of the calculation scheme for RFB

References

Amante, C., Eakins, B., 2009. Etopo1 1 arc-minute global relief model: procedures, data sources and analysis. Technical report, NOAA Technical Memorandum NESDIS NGDC-24.

An, M., Wiens, D.A., Zhao, Y., Feng, M., Nyblade, A.A., Kanao, M., Li, Y., Maggi, A., Lévéque, J.-J., 2015. S-velocity model and inferred Moho topography beneath the Antarctic Plate from Rayleigh waves. J. Geophys. Res.: Solid Earth 120 (1), 359–383.

Argus, D.F., Peltier, W.R., Drummond, R., Moore, A.W., 2014. The Antarctica component of postglacial rebound model ICE-6g_c (VM5a) based on GPS positioning, exposure age dating of ice thicknesses, and relative sea level histories. Geophys. J. Int. 198 (1), 537–563.

Barletta, V.R., Bevis, M., Smith, B.E., Wilson, T., Brown, A., Bordoni, A., Willis, M., Khan, S.A., Rovira-Navarro, M., Dalziel, I., Smalley, R., Kendrick, E., Konfal, S., Caccamise, D.J., Aster, R.C., Nyblade, A., Wiens, D.A., 2018. Observed rapid bedrock uplift in Amundsen Sea Embayment promotes ice-sheet stability. Science 360 (6395), 1335–1339.

Chen, J.L., Wilson, C.R., Blankenship, D., Tapley, B.D., 2009. Accelerated Antarctic ice loss from satellite gravity measurements. Nat. Geosci. 2 (12), 859–862.

Dziewonski, A.M., Anderson, D.L., 1981. Preliminary reference earth model. Phys. Earth Planet. Inter. 25 (4), 297–356.

Farrell, W.E., Clark, J.A., 1976. On postglacial sea level. Geophys. J. R. Astron. Soc. 46 (3), 647–667.

Fretwell, P., Pritchard, H.D., Vaughan, D.G., Bamber, J.L., Barrand, N.E., Bell, R., Bianchi, C., Bingham, R.G., Blankenship, D.D., Casassa, G., Catania, G., Callens, D., Conway, H., Cook, A.J., Corr, H.F.J., Damaske, D., Damm, V., Ferraccioli, F., Forsberg, R., Fujita, S., Gim, Y., Gogineni, P., Griggs, J.A., Hindmarsh, R.C.A., Holmlund, P., Holt, J.W., Jacobel, R.W., Jenkins, A., Jokat, W., Jordan, T., King, E.C., Kohler, J., Krabill, W., Riger-Kusk, M., Langley, K.A., Leitchenkov, G., Leuschen, C., Luyendyk, B.P., Matsuoka, K., Mouginot, J., Nitsche, F.O., Nogi, Y., Nost, O.A., Popov, S.V., Rignot, E., Rippin, D.M., Rivera, A., Roberts, J., Ross, N., Siegert, M.J., Smith, A.M., Steinhage, D., Studinger, M., Sun, B., Tinto, B.K., Welch, B.C., Wilson, D., Young, D.A., Xiangbin, C., Zirizzotti, A., 2013. Bedmap2: improved ice bed, surface and thickness datasets for Antarctica. Cryosphere 7 (1), 375–393.

Harley, S.L., Fitzsimons, I.C.W., Zhao, Y., 2013. Antarctica and supercontinent evolution: historical perspectives, recent advances and unresolved issues. Geol. Soc. Lond. Spec. Publ. 383 (1), 1–34.

Hay, C.C., Lau, H.C.P., Gomez, N., Austermann, J., Powell, E., Mitrovica, J.X., Latychev, K., Wiens, D.A., 2017. Sea level fingerprints in a region of complex earth structure: the case of WAIS. J. Climate 30 (6), 1881–1892.

Jacob, T., Wahr, J., Pfeffer, W.T., Swenson, S., 2012. Recent contributions of glaciers and ice caps to sea level rise. Nature 482 (7386), 514–518.

Kendall, R.A., Mitrovica, J.X., Milne, G.A., 2005. On post-glacial sea level – II. Numerical formulation and comparative results on spherically symmetric models. Geophys. J. Int. 161 (3), 679–706.

Khan, S.A., Sasgen, I., Bevis, M., van Dam, T., Bamber, J.L., Wahr, J., Willis, M., Kjær, K.H., Wouters, B., Helm, V., Csatho, B., Fleming, K., Bjrk, A.A., Aschwanden, A., Knudsen, P., Munneke, P.K., 2016. Geodetic measurements reveal similarities between post-Last Glacial Maximum and present-day mass loss from the Greenland ice sheet. Sci. Adv. 2 (9), e1600931.

Martin-Español, A., King, M.A., Zammit-Mangion, A., Andrews, S.B., Moore, P., Bamber, J.L., 2016. An assessment of forward and inverse GIA solutions for Antarctica. J. Geophys. Res.: Solid Earth 121 (9), 6947–6965.

Milne, G.A., Mitrovica, J.X., 1998. Postglacial sea-level change on a rotating Earth. Geophys. J. Int. 133 (1), 1–19.

Milne, G.A., Mitrovica, J.X., Davis, J.L., 1999. Near-field hydro-isostasy: the implementation of a revised sea-level equation. Geophys. J. Int. 139, 464–482.

Mitrovica, J.X., Gomez, N., Morrow, E., Hay, C., Latychev, K., Tamisiea, M.E., 2011. On the robustness of predictions of sea level fingerprints: On predictions of sea-level fingerprints. Geophys. J. Int. 187 (2), 729–742.

Mitrovica, J.X., Milne, G.A., Davis, J.L., 2001. Glacial isostatic adjustment on a rotating earth. Geophys. J. Int. 147 (3), 562–578.

Mitrovica, J.X., Peltier, W.R., 1991. On postglacial geoid subsidence over the equatorial oceans. J. Geophys. Res.: Solid Earth 96 (B12), 20053–20071.

Mitrovica, J.X., Wahr, J., Matsuyama, I., Paulson, A., 2005. The rotational stability of an

ice-age earth. Geophys. J. Int. 161 (2), 491–506.
Munk, W.H., MacDonald, G.J., 1960. The Rotation of the Earth: A Geophysical Discussion. Cambridge Univ. Press, New York 323 pp.
Nield, G.A., Barletta, V.R., Bordoni, A., King, M.A., Whitehouse, P.L., Clarke, P.J., Domack, E., Scambos, T.A., Berthier, E., 2014. Rapid bedrock uplift in the Antarctic Peninsula explained by viscoelastic response to recent ice unloading. Earth Planet. Sci. Lett. 397, 32–41.
Nield, G.A., Whitehouse, P.L., van der Wal, W., Blank, B., O'Donnell, J.P., Stuart, G.W., 2018. The impact of lateral variations in lithospheric thickness on glacial isostatic adjustment in West Antarctica. Geophys. J. Int. 214 (2), 811–824.
Paulson, A., Zhong, S., Wahr, J., 2005. Modelling post-glacial rebound with lateral viscosity variations. Geophys. J. Int. 163 (1), 357–371.
Peltier, W.R., Argus, D.F., Drummond, R., 2015. Space geodesy constrains ice age terminal deglaciation: The global ICE-6g_c (VM5a) model. J. Geophys. Res.: Solid Earth 120 (1), 450–487.
Peltier, W.R., Drummond, R., 2008. Rheological stratification of the lithosphere: A direct inference based upon the geodetically observed pattern of the glacial isostatic adjustment of the North American continent. Geophys. Res. Lett. 35 (16).
Rignot, E., Bamber, J.L., van den Broeke, M.R., Davis, C., Li, Y., van de Berg, W.J., van Meijgaard, E., 2008. Recent Antarctic ice mass loss from radar interferometry and regional climate modelling. Nat. Geosci. 1 (2), 106–110.
Sasgen, I., Martín-Español, A., Horvath, A., Klemann, V., Petrie, E.J., Wouters, B., Horwath, M., Pail, R., Bamber, J.L., Clarke, P.J., Konrad, H., Drinkwater, M.R., 2017. Joint inversion estimate of regional glacial isostatic adjustment in Antarctica considering a lateral varying Earth structure (ESA STSE Project REGINA). Geophys. J. Int. 211 (3), 1534–1553.
Sasgen, I., Martín-Español, A., Horvath, A., Klemann, V., Petrie, E.J., Wouters, B., Horwath, M., Pail, R., Bamber, J.L., Clarke, P.J., Konrad, H., Wilson, T., Drinkwater, M.R., 2018. Altimetry, gravimetry, GPS and viscoelastic modeling data for the joint inversion for glacial isostatic adjustment in Antarctica (ESA STSE Project REGINA). Earth Syst. Sci. Data 10 (1), 493–523.
Spada, G., Melini, D., Colleoni, F., 2015. Selen v2.9.12. [Software].
Spada, G., Melini, D., Galassi, G., Colleoni, F., 2012. Modeling Sea Level Changes and Geodetic Variations by Glacial Isostasy: The Improved SELEN Code. arXiv:1212.5061 [physics].
Spada, G., Stocchi, P., 2007. SELEN: A Fortran 90 program for solving the "sea-level equation" Comput. Geosci. 33 (4), 538–562.
The IMBIE team, 2018. Mass balance of the Antarctic Ice Sheet from 1992 to 2017. Nature 558 (7709), 219–222.
van der Wal, W., Whitehouse, P.L., Schrama, E.J., 2015. Effect of GIA models with 3d composite mantle viscosity on GRACE mass balance estimates for Antarctica. Earth Planet. Sci. Lett. 414, 134–143.
Whitehouse, P.L., Bentley, M.J., Le Brocq, A.M., 2012a. A deglacial model for Antarctica: geological constraints and glaciological modelling as a basis for a new model of Antarctic glacial isostatic adjustment. Quat. Sci. Rev. 32, 1–24.
Whitehouse, P.L., Bentley, M.J., Milne, G.A., King, M.A., Thomas, I.D., 2012b. A new glacial isostatic adjustment model for Antarctica: calibrated and tested using observations of relative sea-level change and present-day uplift rates. Geophys. J. Int. 190 (3), 1464–1482.
Zhao, C., King, M.A., Watson, C.S., Barletta, V.R., Bordoni, A., Dell, M., Whitehouse, P.L., 2017. Rapid ice unloading in the Fleming Glacier region, southern Antarctic Peninsula, and its effect on bedrock uplift rates. Earth Planet. Sci. Lett. 473, 164–176.